Physics Letters A 175 (1993) 415–420
North-Holland

PHYSICS LETTERS A

Coupled map lattice model for convection

Tatsuo Yanagita [1]
The Graduate University for Advanced Studies, 4-6-7 Minami-Azabu, Minato-ku, Tokyo 106, Japan

and

Kunihiko Kaneko
Department of Pure and Applied Sciences, University of Tokyo, Komaba, Meguro-ku, Tokyo 153, Japan

Received 25 August 1992; revised manuscript received 9 February 1993; accepted for publication 15 February 1993
Communicated by A.R. Bishop

A coupled map lattice model for convection is proposed, which consists of Eulerian and Lagrangian procedures. Simulations of the model reproduce wide-ranged phenomena in Bénard convection experiments: For a small aspect ratio, formation of convective rolls, their oscillation, and many routes to chaos are found, with the increase of Rayleigh number. For a large aspect ratio, spatiotemporal intermittency is observed. For a high Rayleigh number, transition from soft to hard turbulence is confirmed, as is characterized by the temperature distribution change from Gaussian to exponential. The roll formation in a three-dimensional convection is also simulated, which reproduces experiments well.

Rayleigh–Bénard convection (RBC) has always been a typical experiment for chaos, spatiotemporal chaos, pattern formation, and turbulence. For a small aspect ratio, the transition to chaos of the oscillation of convective rolls was studied with the increase of Rayleigh number [1]. For a large aspect ratio, spatiotemporal intermittency (STI) is observed at the transition to turbulence [2]. The process of formation of rolls in a system with a large container gives a prototype for the pattern formation and the slow motion of defects between rolls [3]. For larger Rayleigh number, a transition from soft to hard turbulence was clarified by Libchaber's group [4].

So far, only some of these experimental results (e.g., low-dimensional chaos) are partially reproduced by extensive simulation with the use of the Navier–Stokes equation. We do not have a single simple model which reproduces all the above phenomena as yet. In the present Letter we report a simple coupled map lattice (CML) model which can reproduce all the above phenomena just by the change of aspect ratio, Prandtl number, and Rayleigh number. The agreement with experiments is mostly qualitative, although some quantitative agreements are presented in the STI and in the transition from soft to hard turbulence.

The CML model is one of the most powerful methods to study the dynamics in spatially extended systems [5]. CML modeling is based on the separation and successive operation of procedures which are represented as maps acting on field variables on a lattice. The CML model has been successfully applied as simulators for various physical phenomena [6]. Here we decompose the fluid motion into Eulerian and Lagrangian procedures, to include the advective motion [7].

First we choose a two-dimensional lattice (x, y) with y as perpendicular direction, and assign the velocity field $\boldsymbol{v}^t(x, y)$ and internal energy $E^t(x, y)$ as a field variable at time t. The dynamics of the field consists of Lagrangian and Eulerian parts. The latter part is further decomposed into the buoyancy force, heat diffusion and viscosity, which are carried out by

[1] Present address: Department of Applied Physics, Tokyo Institute of Technology, Meguro-ku, Tokyo 152, Japan.

the conventional CML modeling method [6]. Here we assume that $E^t(x, y)$ is scaled so that its average is roughly 0; in other words, $E^t(x, y)$ takes opposite signs at the top plate and the bottom plate. In the constructing procedures, we assume that $E^t(x, y)$ is associated with the temperature.

For the Eulerian part we notice the following prescriptions: (I) a site with higher temperature receives a force in the upward direction; (II) heat diffusion leads to the diffusion for $E^t(x, y)$; (III) the velocity field $v^t(x, y)$ is also under diffusive dynamics, due to the viscosity; (IV) in an incompressible fluid, the pressure term requires div $\boldsymbol{v}$ to be 0. We do not take this condition here, since the inclusion of pressure requires more complicated modeling. Instead, we borrow a term from compressible fluid dynamics, which brings about this pressure effect, and constrains the div $\boldsymbol{v}$ term from growing to large values. This term is given by the discrete version of grad(div $\boldsymbol{v}$). An "expanded" region with larger div $\boldsymbol{v}$ imposes a force to neighboring lattice points through this term. Combining these dynamics, the Eulerian part is written as the successive operations of the following mappings (hereafter we use the notation for the discrete Laplacian operator: $\Delta A(x, y) = \frac{1}{4}[A(x-1,y)+A(x+1,y)+A(x,y-1)+A(x,y+1)-4A(x, y)]$ for any field variable A):

(i) buoyancy procedure,

$$v_y^*(x, y) = v_y^t(x, y) + \tfrac{1}{2}c[2E^t(x, y) - E^t(x+1, y) - E^t(x-1, y)],$$
$$v_x^*(x, y) = v_x^t(x, y), \tag{1}$$

(ii) heat diffusion,

$$E^t(x, y) = E^t(x, y) + \kappa \Delta E^t(x, y), \tag{2}$$

(iii) viscosity and pressure effect,

$$v_x^t(x, y) = v_x^*(x, y) + \nu \Delta v_x^*(x, y) + \eta\{\tfrac{1}{2}[v_x^*(x+1, y) + v_x^*(x-1, y)] - v_x^*(x, y) + \tfrac{1}{4}[v_y^*(x+1, y+1) + v_y^*(x-1, y-1) - v_y^*(x-1, y+1) - v_y^*(x+1, y-1)]\} \tag{3}$$

and the equation with $x \leftrightarrow y$.

Successive operation of the above three parallel procedures completes the Eulerian scheme. The Lagrangian scheme expresses the advection of velocity and temperature. We set a quasi-particle on each lattice site (x, y). The particle has a velocity $\boldsymbol{v}(x, y)$ and moves to $(x+\delta x, y+\delta y)$ by the Lagrangian scheme, where $\delta x = v_x(x, y)$, $\delta y = v_y(x, y)$. All field variables (velocity and internal energy) are carried by this particle. Since there is no lattice point at the position $(x+\delta x, y+\delta y)$ generally, we allocate the field variable on its four nearest neighbor sites. The weight of this allocation is given by the lever rule; $(1-\delta x)(1-\delta y)$, $\delta x(1-\delta y)$, $(1-\delta x)\delta y$, and $\delta x \delta y$ for the sites $([x+\delta x], [y+\delta y])$, $([x+\delta x]+1, [y+\delta y])$, $([x+\delta x], [y+\delta y]+1)$ and $([x+\delta x]+1, [y+\delta y]+1)$ respectively, with $[z]$ as the maximal integer smaller than z.

The total dynamics of our model is given by successive applications of the above procedures; $\{\boldsymbol{v}^t(x, y), E^t(x, y)\} \to \{\boldsymbol{v}^{a*}(x, y), E^t(x, y)\} \to \{\boldsymbol{v}^t(x, y), E^t(x, y)\}$ - (Lagrangian) $\to \{\boldsymbol{v}^{t+1}(x, y), E^{t+1}(x, y)\}$ [#1]. This completes one step of dynamics.

For the boundary, we choose the following conditions. (I) Top and bottom plates: assuming the allocation of E to temperature, we choose the boundary condition $E(x, 0) = \delta T = -E(x, N_y)$. For the velocity field we have used either a fixed boundary or free boundary. For the Lagrangian scheme, we use a fixed or reflection boundary. (II) Side wall at $x=0$ and $x=N_x$: we use either fixed, reflective, and periodic boundary conditions. Hereafter we mostly choose the fixed boundary for top and bottom plates and the periodic boundary condition for the x-direction. Changing to a fixed boundary at the wall alters our velocity pattern (for a small size), but most of the transition sequence of the patterns remain invariant.

Basic parameters in our model (and in experiments) are Rayleigh number (proportional to δT), Prandtl number (ratio of viscosity to heat diffusion, ν/κ), and aspect ratio (N_x/N_y). Here we study in detail the dependence of the convection pattern on the Rayleigh number and the aspect ratio. For simulations we take the diffusion coefficient η as $\frac{1}{3}\nu < \eta \leqslant \nu$ [8], although our results are reproduced, as far as η is the same order of ν, where div $\boldsymbol{v}$ is kept small numerically.

For small Rayleigh number, we have a steady con-

[#1] The order of operations of procedures is not important. Models with different orders give essentially the same phenomenology.

vective flow. Few rolls are formed, the number of which increases with δT and the aspect ratio. At small aspect ratio, these rolls start to oscillate periodically in time, with the increase of δT. If the Prandtl number is small, we have observed period doubling bifurcation to chaos with the further increase of δT. Here, we note that the doubling is interrupted after a finite number of times (up to period 4 or 8). In the experimental observation, it is believed that noise induces such imperfect bifurcation. In our simulation, high dimensional dynamics plays the role of a generator of "noise", which, we believe, is the origin of the interruption of a doubling sequence in real fluid systems. If the Prandtl number is larger, the onset of chaos occurs through a quasiperiodic state (two-dimensional torus), in agreement with the experimental observation of the route to chaos [1].

For a large aspect ratio, many steady convective rolls are formed. The number of rolls increases with δT. With the increase of δT, the rolls start to oscillate periodically (all the rolls have the same frequency). As δT is further increased, the collective oscillatory behavior becomes unstable. Laminar roll motion and turbulent motion coexist in spacetime as is shown in fig. 2.

We have measured the distribution of the size of a laminar region to characterize the STI transition [5]. The distribution of the spatial length of laminar domains is given in fig. 3. It clearly shows the power law distribution at the STI transition, while the distribution decays exponentially when the Rayleigh number is larger. These results agree with the observation in the RBC experiments with a large aspect ratio [2]. The exponent of the power law distribution is 2.0 ± 0.2 from our simulation, which agrees with experimental results [2].

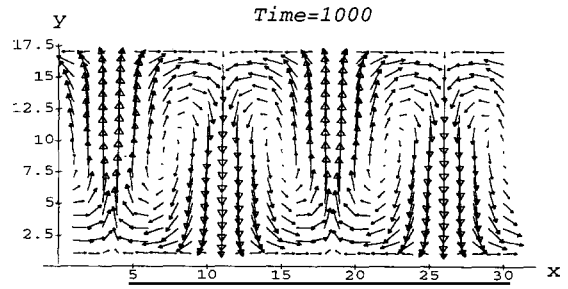

Fig. 1. Snapshot of convective roll pattern for our CML model. The velocity field of our CML model is shown for time step $t=300$. $N_x=30$, $N_y=17$, $\nu=0.2$, $\kappa=0.4$, and $\delta T=0.1$.

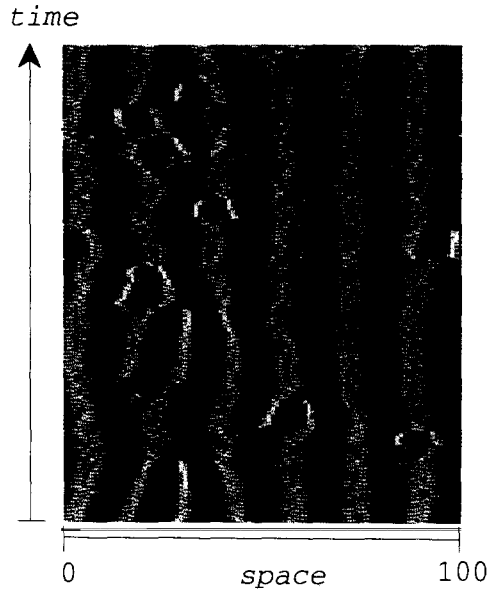

Fig. 2. Spatiotemporal pattern of velocity field v_y. Successive changes of $v_y(x, \frac{1}{2}N_y)$ are plotted in spacetime, with the use of a gray scale with black and white indicating $v_y=\pm 0.75$ respectively. $N_x=100$, $N_y=17$, $\nu=0.2$, $\kappa=0.4$, $\eta=0.3$, and $\delta T=1.2$.

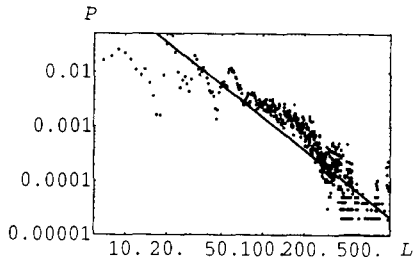

Fig. 3. Log-log plot of the probability distribution for the length of the laminar domain. The distribution shows a power law at the onset of STI. $N_x=850$, $N_y=17$, $\nu=\kappa=0.2$ and $\delta T=0.1$. As δT is increased, the exponential distribution replaces the power law.

For larger δT, hot and cold plumes start to appear. Plumes in our model are defined as isolated sets of a few connected lattice points with larger or smaller energy E than their neighbors. If δT is not large enough, hot plumes cannot reach the opposite plate (and vice versa for cold plumes). A hot layer is connected near the bottom plate. The boundary layer still remains. With the increase of δT (>6.0), the layer splits into disconnected regimes, and plumes

can reach the opposite plate (see fig. 4 for the contour plot of $E(x, y)$). A similar change of convective pattern is found by Libchaber's group, where each state is termed as soft (for the former) and hard turbulence. According to their experiment, the temperature distribution (in the middle of the container) is Gaussian in soft turbulence, and exponential in hard turbulence [4]. We have measured the distribution of $E(x, \frac{1}{2}N_y)$ by sampling over 10^5 time steps, and over the horizontal position x (note the periodic boundary condition for the side wall). The distribution is plotted in fig. 5, which shows the transition from Gaussian to exponential.

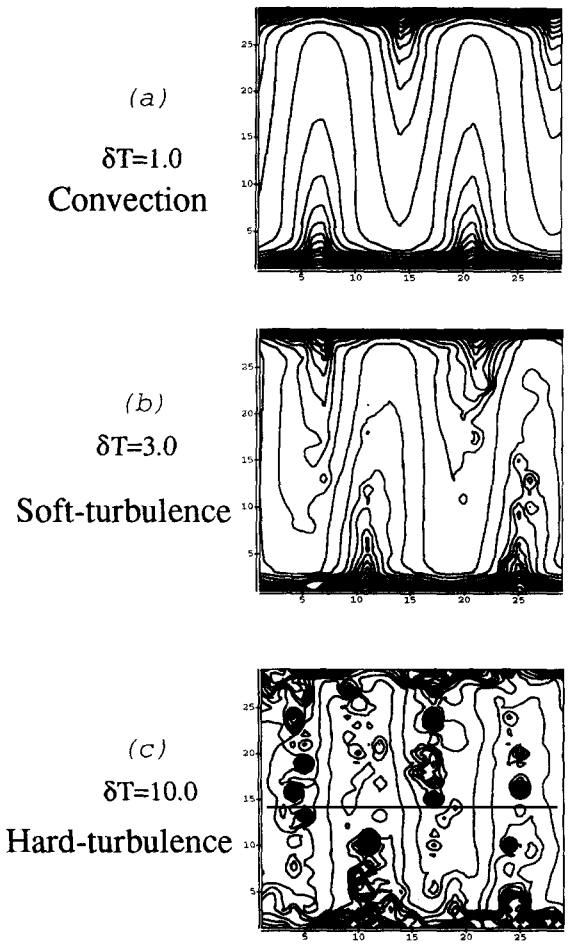

Fig. 4. Snapshot of equi-energy (equi-temperature) contour, plotted with 30 levels for $E=-\delta T$ to δT. $N_x=N_y=30$, $\nu=\kappa=0.2$. (a) $\delta T=1.0$ (b) $\delta T=3.0$ (c) $\delta T=10.0$.

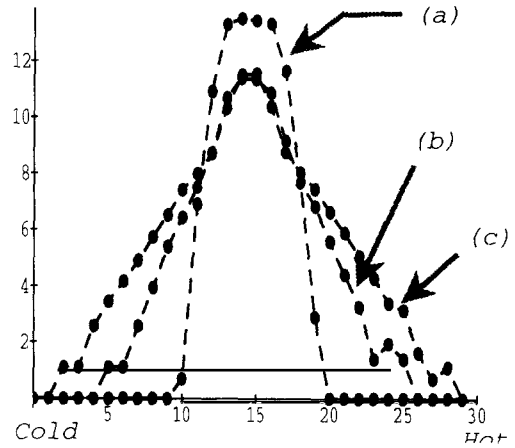

Fig. 5. The distribution of $E(x, \frac{1}{2}N_y)$ sampled over time and x. Three examples are overlayed with increasing Rayleigh number. $N_x=N_y=30$, and $\nu=\kappa=0.2$.

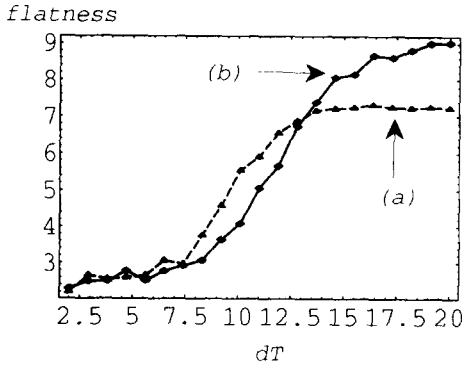

Fig. 6. Rayleigh number dependence of the flatness $\langle (E-\langle E\rangle)^4\rangle\langle (E-\langle E\rangle)^2\rangle^{-2}$ of the temperature distribution. For a low Prandtl number ((a) $\nu=0.2$ and $\kappa=0.5$), the flatness is raised from 3 to 6 with the increase of δT, while it is raised up to 12 for a high Prandtl number ((b) $\nu=0.2$ and $\kappa=0.3$). Furthermore, the plateau around 3 (in the soft turbulent regime) gets narrower by decreasing the Prandtl number.

We have computed the flatness of the distribution $(\langle [\delta E(N_x, \frac{1}{2}N_y)]^4\rangle\langle [\delta E(N_x, \frac{1}{2}N_y)]^2\rangle^{-2}$ with $\delta E = E-\langle E\rangle$) (fig. 6). For a low Prandtl number, the flatness rises from 3 to 6 with the increase of δT, in agreement with experiments. For the high Prandtl number regime, on the other hand, the flatness rises continuously up to 12. We also note that the plateau around flatness 3 (in the soft turbulence region) gets narrower with the decrease of the Prandtl number. The Prandtl number dependence of the flatness is

our prediction here, which, we hope, will be confirmed in future experiments.

Our CML model provides the first simple model for the soft–hard turbulence transition [#2]. Besides the above quantitative characterization, our observation of the energy pattern also suggests that this transition is associated with the percolation of plumes at the bottom plate.

The extension of our model to three dimensions is quite straightforward. We have simulated a three-dimensional convection in rectangular and cylinder containers, taking a fixed boundary at the wall. Starting from an almost homogeneous field, rolls are formed locally within short time steps, while the slow motion of the defects between locally aligned rolls is observed later, over long time steps, as has been found in experiments [3] (see fig. 7). The domain size of aligned rolls increases so slowly that the irregular motion of defects remains over long time steps. If the Rayleigh number is larger, these defects form cellular structures as in fig. 7c.

In summary, we have proposed a CML model for RBC, by introducing a Lagrangian scheme, where the advective motion is expressed by quasi-particles. Our model reproduces almost all phenomenology in experiments; a steady convective flow, roll formation process, periodic oscillation of rolls, bifurcation to chaos, and STI. In particular, the transition from soft to hard turbulence is confirmed, where the temperature distribution changes its shape from Gaussian to exponential, in agreement with experimental observation.

Some, still, may doubt our CML approach, just because our model is not derived from the Navier–Stokes equation. Our standpoint here is that the salient features in convection are irrespective of the details of models. Such features form universality classes. For the understanding of the complex phenomena, the prediction of universality classes by a model constructed from simple procedures is important. Our model suggests that the soft–hard transition originates in the percolative behaviour of plumes. This allocation forms the basis of universality, e.g., the universal change of the temperature distribution. The essence of the transition does not

[#2] For an abstract CML model for plumes, see also ref. [9].

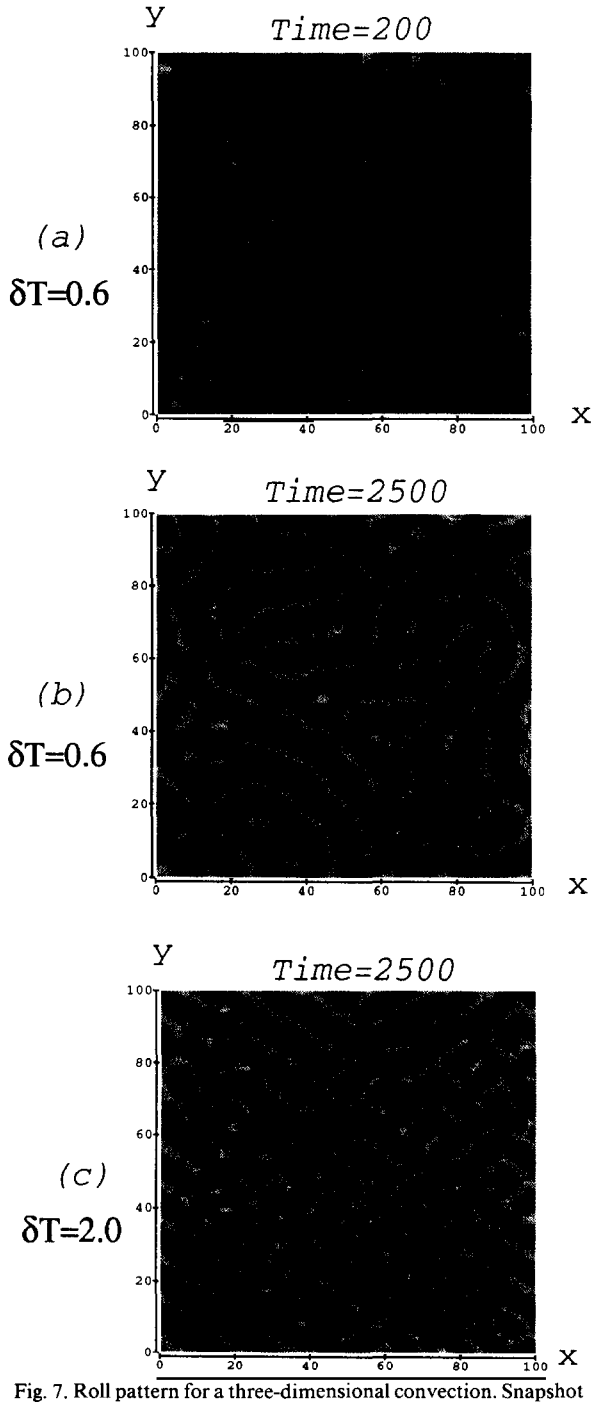

Fig. 7. Roll pattern for a three-dimensional convection. Snapshot of the perpendicular velocity v_z at the middle plate $(x, y, \frac{1}{2}N_z)$ is shown with the use of a gray scale with black and white indicating $v_z = \pm V_{max}$ respectively. The lattice size is $(N_x, N_y) = 100 \times 100$ (horizontal), and $N_z = 9$. $\nu = \kappa = 0.2$. $\delta T = 0.6$ for (a) and (b). (a) Time step 200, $V_{max} = 0.07$, (b) time step 2500, $V_{max} = 0.2$, (c) time step 2500. $\delta T = 2.0$ and $V_{max} = 0.6$.

depend on the details of models, as long as they belong to the same universality class.

It should be mentioned that our Lagrangian procedure is also useful to construct a CML model for a shear flow, Kármán vortex and its collapse. Inclusion of rotation in the convection is rather straightforward. Another important extension of our CML model is the inclusion of phase transition dynamics, as is seen in boiling [10] and cloud dynamics. These examples will be reported elsewhere.

We would like to thank M. Sano, S. Adachi and J. Suzuki for useful discussions. This work is partially supported by Grant-in-Aids for Scientific Research from the Ministry of Education, Science, and Culture of Japan, and by a cooperative research program in The Institute for Statistical Mathematics.

References

[1] J.P. Gollub and S.V. Benson, J. Fluid Mech. 100 (1980) 449;
J. Maurer and A. Libchaber, J. Phys. (Paris) 41 (1980) L515.
[2] S. Ciliberto and P. Bigazzi, Phys. Rev. Lett. 60 (1988) 286;
F. Daviaud, M. Dubois and P. Berge, Europhys. Lett. 9 (1989) 441.
[3] C.W. Meyer, G. Ahlers and D.S. Cannell, Phys. Rev. Lett. 59 (1987) 1577.
[4] F. Heslot, B. Castaing and A. Libchaber, Phys. Rev. A 36 (1987) 5870;
M. Sano, X.Z. Wu and A. Libchaber, Phys. Rev. A 40 (1989) 6421.
[5] K. Kaneko, Prog. Theor. Phys. 72 (1984) 480; 74 (1985) 1033; Physica D 34 (1989) 1; 36 (1989) 60.
[6] K. Kaneko, in: Formation, dynamics, and statistics of patterns, eds. K. Kawasaki, A. Onuki and M. Suzuki (World Scientific, Singapore, 1990).
[7] A. Shinozaki and Y. Oono, Forma 4 (1989) 15.
[8] L.D. Landau and E.M. Lifshitz, Fluid mechanics (Pergamon, Oxford, 1959) §15.
[9] M.H. Jensen, Phys. Rev. Lett. 62 (1989) 1361.
[10] T. Yanagita, Phys. Lett. A 165 (1992) 405.